Materials Advances

ROYAL SOCIETY OF CHEMISTRY

PAPER

View Article Online
View Journal | View Issue

Cite this: *Mater. Adv.*, 2020, 1, 1273

Ag and Mn-doped mesoporous bioactive glass nanoparticles incorporated into the chitosan/gelatin coatings deposited on PEEK/bioactive glass layers for favorable osteogenic differentiation and antibacterial activity†

Aneeqa Nawaz, Shaher Bano, Muhammad Yasir, Abdul Wadood and Muhammad Atiq Ur Rehman *

Received 18th May 2020,
Accepted 1st July 2020

DOI: 10.1039/d0ma00325e

rsc.li/materials-advances

Bioactive and antibacterial coatings were developed and characterized in this study. Chitosan/gelatin/Ag–Mn doped mesoporous bioactive glass nanoparticles (Ag–Mn MBGNs) composite coatings (of 5–6 μm thickness) were deposited using electrophoretic deposition (EPD) on PEEK/bioactive glass (BG) layers (of 60–70 μm thickness), which had been deposited by EPD onto stainless steel. The chitosan/gelatin/Ag–Mn MBGNs composite coatings deposited on PEEK/BG layers were optimized by the Taguchi design of experiment (DoE) approach; the resulting microstructure, composition, *in vitro* bioactivity, antibacterial activity, and cytocompatibility were investigated. Scanning electron microscopy (SEM) images confirmed the deposition of Ag–Mn MBGNs on the surface of PEEK/BG layers. Energy dispersive spectroscopy (EDX) confirmed the presence of Mn and Ag, which were embedded in chitosan/gelatin (top layer). The presence of BG particles in the PEEK/BG layer and Ag–Mn MBGNs in the top layer allows the multi-structured coatings to form apatite like crystals upon immersion in simulated body fluid (SBF). Moreover, the release of silver ions from the top layer provided an antibacterial effect against *Escherichia coli* and *Staphylococcus carnosus*.

1. Introduction

The current challenge in the development of orthopedic implants is to minimize the risk of infections. The average population suffering from implant-related infection is increasing.[1] Therefore, there is a pressing need for the development of antibacterial and bioactive implants (in particular orthopedic implants). The main reason for implant-related infection is the formation of biofilm on the surface of the implant.[1,2] The biofilm is resistant to the immune system of the body, which may result in a lack of cellular interaction between the implant and the bone.[2,3] The biofilm starts to develop after a few hours of implantation. To prevent the formation of biofilm implants are often impregnated with gentamicin before implantation.[3] This strategy is certainly useful, but the availability of drugs at the targeted site cannot be ensured for a longer period. To address this, antibacterial drugs are loaded in the polymer matrix, which allows the controlled release of the drug for longer periods.[4–6] However, the widespread use of antibiotics has led to the development of bacterial strains that are resistant to the immune system of the body and to the antibiotics.[1,7] To address this issue, several metallic ions have been investigated to provide an antibacterial effect against a wide spectrum of bacteria, for example, silver, copper, zinc, *etc.*[8–11]

Mesoporous bioactive glass nanoparticles (MBGNs) have shown promising bioactivity and can enhance the proliferation of osteoblast-like cells (MG-63).[12] MBGNs based on SiO_2–P_2O_5–Cao have demonstrated promising properties for the local delivery of therapeutically active ions.[13,14] MBGNs can be doped with several metallic ions to provide a therapeutic effect.[15] For example, Westhauser *et al.*[16] and Nawaz *et al.*[8] doped MBGNs (composition in mol%: $50SiO_2$–$10P_2O_5$–40Cao) with Mn (composition in mol%: $50SiO_2$–$10P_2O_5$–35Cao–5MnO). The results have shown that 5 mol% addition of MnO in MBGNs supported osteogenic differentiation and enhanced the upregulation of genes encoding for extracellular matrix proteins.[16] Aiah *et al.* doped MBGNs with silver ions and found that Ag-MBGNs were bioactive and antibacterial against Gram-positive and Gram-negative bacteria.[17] It has been reported in the literature that MBGNs constitute an attractive vector for therapeutically active

Department of Materials Science and Engineering, Institute of Space Technology Islamabad, 1, Islamabad Highway, Islamabad, 44000, Pakistan.
E-mail: atique1.1@hotmail.com

† Electronic supplementary information (ESI) available. See DOI: 10.1039/d0ma00325e

ions since they exhibit an intrinsic pro-osteogenic potential that can be improved by the incorporation of therapeutically active ions.[16] The properties and the synthesis of sol–gel derived MBGNs have been reviewed by Kai *et al.*[18]

Chitosan is a well-known biocompatible natural biopolymer, which can improve the cellular interaction between the implant and the bone.[6] However, chitosan has shown rapid degradation in the biological environment. To improve the stability of chitosan, gelatin can be incorporated into chitosan.[6,19] Gelatin is a polypeptide which has the properties of the extracellular matrix.[20,21] Gelatin when mixed with chitosan forms a polyelectrolyte complex, which is mechanically robust.[22] The properties of chitosan/gelatin (labeled as CG) coatings have recently been reviewed by Avcu *et al.*[6] The mixture of CG can also be used as a matrix to provide the controlled release of metallic ions.[6,19] For example, CG/MBGNs doped with silver can show enhanced bioactivity due to the release of calcium and phosphate ions and an antibacterial effect due to the release of silver ions.[19] The slow degradation of the CG matrix will also be useful for the controlled release of silver, which will reduce the potential cytotoxic effect associated with excessive release of silver ions. Moreover, the release of Mn ions will be beneficial for the attachment and proliferation of osteoblast-like cells.[16]

Polyetheretherketone (PEEK)/bioactive glass (BG) coatings have widely been employed in the last few years due to their excellent mechanical stability and enhanced bioactivity.[7,23–25] Furthermore, the robust PEEK/BG (labeled as PB) layers have also been shown to improve the corrosion resistance of stainless steel substrates.[26] The intrinsic roughness of PB layers has been used in the literature to infiltrate biologically active molecules along with different drugs to improve the biocompatibility and to provide the antibacterial effect.[26–28] Accordingly, in this study, we have developed multi-structured coatings consisting of CG/Mn–Ag MBGNs (labeled as CGAgMnB) layers deposited on PB layers for the first time. In our previous study, we deposited silver nanocluster–silica composite coatings on PB layers. The coatings were antibacterial and bioactive but did not assist cell spreading and proliferation due to the hydrophilic nature of silver nanocluster–silica composite coatings.[1] Therefore, we have developed the top layer consisting of CGAgMnB which supports the proliferation of osteoblast cells due to favorable surface chemistry and wettability. The toxic effect associated with silver was mitigated with the addition of Mn in the network of glass. This is the first study to report the deposition of co-doped MBGNs for favorable osteogenic differentiation and antibacterial activity. The bottom layer as in our previous study has been shown to provide bioactivity, wear resistance, and corrosion resistance.[29]

Electrophoretic deposition (EPD) is a widely adopted low-temperature processing technique for the deposition of biomaterials.[5] EPD has been utilized for achieving uniform films of various biopolymers embedded with bioceramics and biomolecules. However, the mechanism controlling the co-deposition of biopolymers and bioceramics is not well-explained in the literature.[29] In principle, the particles intended to be deposited are charged depending upon their pH, and then the charged particles/molecules migrate towards the oppositely charged electrode.[30] EPD has recently been studied to deposit chitosan/BG/Lawson on PB layers (the product is multi-structured coatings).[26] Therefore, EPD is a suitable technique for the deposition of homogeneous multi-structured coatings for biomedical applications.

In this study, we have obtained CGAgMnB layers on PB layers *via* EPD. PB layers were intended to provide bio-stable layers with enhanced bioactivity. On the other hand, CGAgMnB is expected to improve the cellular attachment and antibacterial effect. Fourier transform infrared spectroscopy (FTIR) analysis confirmed the deposition of CG on PB layers. Energy dispersive X-ray (EDX) analysis confirmed the deposition of Ag–Mn MBGNs on PB layers. Multi-structured coatings developed hydroxyapatite crystals upon immersion in simulated body fluid (SBF). The release of silver from the multi-structured coatings allowed the development of the zone of inhibition against Gram-positive and Gram-negative bacteria. Multi-structured coatings were biocompatible to osteoblast-like cells.

2. Materials and methods

2.1 Materials

45S5 BG (Schott AG™, Germany) of nominal composition 45 wt% SiO_2, 24.5 wt% Na_2O, 24.5 wt% CaO, and 6 wt% P_2O_5[31] and with a mean particle size of 4 μm and PEEK powder (704 XF, Victrex™) with a mean particle size of 10 μm were used. The relevant size of the particles was adopted from the previous study.[29] The Ag–Mn doped MBGNs with a diameter of ~180 nm and 8 nm pore diameter were synthesized *via* a modified Stöber method, as reported in ref. 16. The nominal composition of as-synthesized MBGNs was $50SiO_2$–$10P_2O_5$–40Cao (mol%) and that of Ag–Mn MBGNs was $50SiO_2$–$10P_2O_5$–34Cao–5MnO–1Ag (mol%).

2.2 PEEK/BG suspension (first layer)

For deposition of the first layer (PB) a stable suspension of PEEK and BG particles was prepared, following the previous studies.[7,25] To prepare the stable suspension, firstly 6.67 wt% BG and 13.34 wt% monohydrate citric acid (VWR International) were mixed in a beaker with ethanol (EMSURE® Merck KGaA, 99–100% purity, denatured with 1% methyl ethyl ketone for analysis). After 3 h of ultrasonication, the particles were dispersed homogeneously in the suspension. Afterward, 2 wt% PEEK was added into the prepared suspension and the pH was adjusted to ~4.5.

2.3 EPD of PEEK/BG (first layer)

AISI 316L stainless steel foil (ISO 9445-1, ThyssenKrupp AG) was cut into 1.5 (width) × 3 (length) cm electrodes. Afterward, the electrodes were cleaned with a mixture of ethanol and acetone (both from VWR International) and then rinsed with deionized water (taken from ELGA DV 25 Purelab option R7BP). 316L stainless steel (SS) was used as the substrate material because of its low cost and the coatings deposited on SS *via* EPD

can be converted on Mg, Ti, and other metallic substrates. Therefore, the results achieved here on SS will also be valid for other metals and alloys. The stainless steel substrate and the counter electrode were immersed in the prepared PB suspension. The distance between the substrate and the counter-electrode was kept at 0.5 cm, the voltage was 80 V (EX735M Multi-Mode PSU 75 V/150 V 300 W power supply device and a 1906 High-Resolution Computing Multimeter both from Thurlby Thandar Instruments Limited) and the deposition time was 90 s for the deposition of the PB composite on 316L SS, following the previous studies on EPD of PB.[7,25] After each coating, the suspension was magnetically stirred to ensure that the suspension remains stable. PB coatings were dried at ambient temperature for 12 h and then sintered in a furnace (Nabertherm™ GmbH) for 30 min at 375 °C with a heating and cooling rate of 2 °C min^{-1}.

2.4 Chitosan/gelatin/Ag–Mn MBGNs suspension (second layer)

CG solution was prepared according to the procedure discussed in our previous study.[19] CG was mixed in the volumetric ratio of 1 : 1 (50 vol% chitosan : 50 vol% gelatin). The volumetric concentration of chitosan and gelatin was optimized in our previous study by applying the Taguchi design of experiment (DoE) approach.[19] Afterward, a portion of 2 g L^{-1} Ag–Mn MBGNs was added into the prepared CG solution (the concentration of Ag–Mn MBGNs in the CG matrix was optimized by the DoE approach, data not shown here).

2.5 EPD of chitosan/gelatin/Ag–Mn MBGNs on PEEK/BG layers (second layer)

The optimum parameters for the deposition of CGAgMnB on PB layers were chosen according to the Taguchi DoE approach (data not shown here). The optimum EPD parameters were as follows: the inter-electrode distance of 0.5 cm, an applied voltage of 30 V, and a deposition time of 5 min. The details of the components of the suspension and EPD parameters are presented in Table 1.

2.6 Characterization of the coatings

Optical validation was done by SEM (LEO 435 VO by Carl Zeiss AG, 5–15 kV). The samples were sputtered before SEM analysis using a sputter coater (Q150/S by Quorum Technologies). Elemental composition (qualitative) was investigated by EDX (same device and preparation as for SEM). The crystal structure of the coatings was determined by X-ray diffraction analysis (XRD, D8 Advance, Bruker™). The contact angle was measured using a drop shape analyzer (DSA40 by Krüss GmbH) using deionized water; for each set of coatings 10 readings were taken and mean values were reported along with the standard deviation. A laser profilometer (UBM™, ISC-2) was used to determine the surface roughness of the coated samples. A scanning velocity of 400 points per second and a measurement length of 5 to 7 mm were used in the UBM™ software to calculate the average roughness (R_a). The relevant chemical bonds were determined by FTIR (Nicolet 6700 by Thermo Scientific) within the wavelength of 400–4000 cm^{-1} at a resolution of 4 cm^{-1}. The stability of the suspension was defined by ζ-potential (nano ZS equipment by Malvern Instruments) measurements.

2.7 *In vitro* bioactivity studies

In vitro bioactivity studies were done by immersing the samples in simulated body fluid (SBF), which was prepared according to ref. 32. Three samples for each type of coating were immersed in 50 mL of SBF and then incubated in a shaking incubator at 37 °C for 1, 3, 7, 14, and 21 days. After taking out the sample at each time point the sample was subjected to SEM, EDX, XRD and FTIR analysis to determine the bioactivity of the coatings.

2.8 Antibacterial study

The ability of the multi-structured coatings (CGAgMnB coatings on PBG layers) to inhibit the growth of bacteria was characterized by the Inhibition halo test, as discussed in ref. 26. To conduct the inhibition halo test the PB coating was used as a control sample. The samples to be used for the inhibition halo test were sterilized for 1 hour under UV light. The agar plates were filled with 20 mL of agar. Afterward, 20 μL of LB-media inoculated separately with *Escherichia coli* and *Staphylococcus carnosus* was added on the top of the agar. The optical density of LB-media after inoculation was kept at 0.015 (OD_{600}). The sterilized multi-structured coatings and control samples were placed on the agar plates inoculated with the bacteria. Finally, agar plates inoculated with bacteria were incubated at 37 °C for 24 hours. After the incubation time the agar plates were taken out and digital images were taken. The obtained digital images were then imported to 'ImageJ' and the zone of inhibition was measured for the multi-structured coatings against

Table 1 Summary of the key EPD parameters and suspension related properties for CGAgMnB composite coatings on the PB layer

Suspension related properties		EPD process parameters	
Chitosan type	Medium molecular weight with 75–85% deacetylation degree	Appl. voltage (V)	30
Chitosan conc. (g L^{-1})	0.5	Deposition time (min)	5
Gelatin conc. (g L^{-1})	1	Inter-electrode distance (mm)	5
Chitosan : gelatin (vol.)	1 : 1	Substrate; a counter electrode	PEEK/BG; 316L SS
Ag–Mn MBGNs	(Mean size: 180 nm) composition in mol%: $50SiO_2$–$10P_2O_5$–34Cao–5MnO–1Ag	Coating thickness	~70 μm (multilayer coatings)
Ag–Mn MBGNs (g L^{-1})	2	Zeta pot. and pH	+33 ± 5 mV and pH 4.2
Charging agent	Acetic acid (1 vol%)		
Suspension solvent	79 vol% eth., 20 vol% distilled water		

both types of bacteria. The test was repeated three times and the standard deviation was reported along with the mean values.

2.9 *In vitro* cellular studies

The human osteosarcoma MG-63 cell line (Sigma Aldrich) was used to investigate the *in vitro* cytocompatibility of the coatings, while PB and tissue culture plate (TCP) were used as controls. To perform cell studies PB and CGAgMnB coatings on PB layers were deposited on disc shaped 316L SS substrates having a diameter of 13.6 mm. *In vitro* cellular studies were conducted by the WST-8 assay. The morphology of the cells attached to the surface of the coatings was examined by fluorescence microscopy. The complete *in vitro* cellular studies were according to the procedure mentioned in ref. 29.

3. Results and discussion

3.1 Morphology of the synthesized mesoporous bioactive glass nanoparticles

The Ag–Mn MBGNs were synthesized by a modified Stöber method. Fig. 1 shows that the particle size of the as-synthesized Ag–Mn MBGNs is ~180 nm, with small pores inside the particles. Fig. 1A shows that the particles are spherical in shape and well dispersed. The porosity of the particles is intrinsic to the Stöber method. Ideally, the particles should be circular to improve the flow properties when in contact with the physiological environment. The synthesized Ag–Mn MBGNs were incoporated in the CG matrix. Thus, variations in the morphology of as-synthesized particles should not impact the final properties of the deposited films. The slight variation in the morphology of the as-synthesized particles from being exactly spherical may be due to the minor changes in pH or temperature during synthesis, as well as in the concentration of ammonia, H_2O, and TEOS in the solution.[8]

3.2 Stability of the suspension

The stability of the suspension is one of the key parameters to determine the quality of the deposits formed during the EPD. For instance, the smaller size particles improve the stability of the suspension; on the other hand, if the suspension contains larger size particles, additional agitation is necessary.[30] ζ-Potential is a function of pH of the suspension, and adjusting the pH to a certain value will result in a higher value of zeta potential and will lead to a stable suspension.[6] The pH of the PB suspension prepared in this study was ~4.5, and ζ-potential at this value of pH was 12 ± 2 mV, which correlates with previous research.[25] The CGAgMnB suspension showed a ζ-potential of 33 ± 5 mV at a pH value of 4.2. Since the value of ζ-potential is positive, cathodic deposition is anticipated. A high ζ-potential prevents the particles from agglomerating due to increasing retraction forces between the particles and leads to a higher density of packing in the coating.[30] The stability of the CG/BG suspension was recently investigated in detail by Ur Rehman *et al.*[19] Based on the previous study it was hypothesized that the positively charged CG complex will encapsulate the Ag–Mn MBGNs, thus leading to the overall positive charge. Upon the application of the electric field, CGAgMnB will migrate towards the cathode.[19,33]

3.3 PEEK/BG composite coatings on 316L SS

Fig. 2(A) and (B) are the SEM images of PB composite coatings. Fig. 2A shows that the BG particles are uniformly embedded in the PEEK matrix. PB composite coatings were homogeneous and the coating thickness was measured to be 60–70 μm (Fig. 2B). The relative amounts of PEEK and BG in the obtained PB composite coatings have been optimized in our previous studies.[25] According to the results of our previous study, the total weight of the composite coatings was attributed to 75 wt% BG and 25 wt% PEEK.[25] Moreover, it was observed that the inner portion of the coatings, *i.e.* closer to the substrate, was densely packed in comparison to the outer portion of the coatings (Fig. 2B). The reason could be that the smaller size PEEK and BG particles were deposited first followed by larger size particles. The smaller size particles can be packed closely thus leading to higher density near the substrate. These results are in agreement with the literature.[25]

The PB layer was intended to provide wear resistance, corrosion resistance, and bioactivity. Our recent study confirmed that the PB composite coatings can offer strong resistance against corrosion in the physiological environment. Moreover, PB composite coatings showed good wear resistance and scratch resistance at the implantation load. PB showed excellent adhesion strength with the 316L SS substrate. The PB layer is bio-stable and will remain on the surface of the substrate even after exposure to the physiological environment.[29]

3.4 Chitosan/gelatin/Ag–Mn MBGNs coatings on 316L SS

Fig. 3 shows the SEM images of the CGAgMnB coating deposited on the 316L SS substrate *via* EPD. The EPD parameters were an

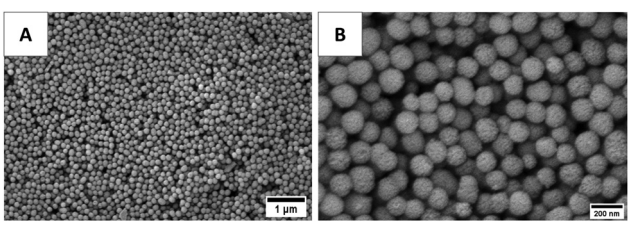

Fig. 1 SEM images showing the morphology of as-synthesized Ag–Mn MBGNs: (A) image at low magnification and (B) image at higher magnification.

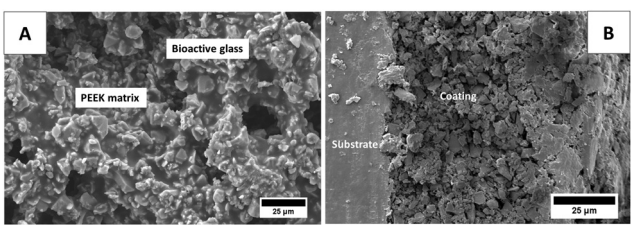

Fig. 2 SEM images showing the morphology of the PB composite coatings after the sintering process: (A) surface image and (B) image at the cross-section.

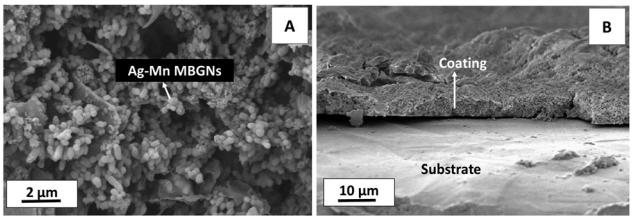

Fig. 3 SEM images showing the CGAgMnB coatings deposited on 316L SS *via* EPD: (A) image of the top surface and (B) image at the cross-section.

applied voltage of 30 V and a deposition time of 5 minutes and the concentration of Ag–Mn MBGNs in the CG solution was 2 g L^{-1}. Fig. 3A shows that the CGAgMnB coatings cover the surface of the 316L SS substrate. However, the pores of ~2 μm were observed in the composite coatings. The Ag–Mn MBGNs were seen to be agglomerated at a few sites in Fig. 3A. It has been reported in the literature that it is difficult to prevent the agglomeration of the nanoparticles in the EPD process (if agglomeration force combined with the applied electrical field is higher than the retraction force, these particles could fuse). However, qualitatively the extent of agglomeration was not substantial to affect the homogeneity of the coatings. Fig. 3B shows that the thickness of the CGAgMnB coatings is ~4 μm. A similar coating thickness for CG/BG has been reported in the literature. The main purpose of the CGAgMnB coating is to provide an antibacterial effect in the multi-structured coating system. Furthermore, the CG matrix is expected to contribute to favorable osteogenic differentiation and proliferation.

3.5 Chitosan/gelatin/Ag–Mn MBGNs composite on PEEK/BG layers

The deposition of the CGAgMnB composite on PB layers was optimized *via* the Taguchi design of experiment (DoE) approach. The DoE approach elucidated that the optimum EPD parameters in terms of deposition yield and homogeneity of the deposited coatings were a deposition voltage of 30 V and a deposition time of 5 min, and the concentration of Ag–Mn MBGNs was 2 g L^{-1}.

SEM and EDX analysis. Fig. 4A and B elucidate that the top layer (CGAgMnB) infiltrated in the porous structure of the PB layer (bottom layer). It is observed that the roughness of the PB layer (R_a = ~2 μm and R_z = 10 μm) varies across the surface. Therefore, the top layer shows complete infiltration at some sites whereas at some sites, the top layer is partially infiltrated. It was hypothesized that the less deep valleys were completely infiltrated with the top layer. In contrast, more deep valleys were not infiltrated completely. Thus, preserving the roughness of the bottom PB layer (Fig. 4B) may lead to enhanced osteogenesis and osteoproduction. Furthermore, Ag and Mn-doped particles will be available in the deep valleys of the bottom layer. Therefore, the contact of these particles with the physiological environment will be delayed and the release of metallic ions from the mesoporous particles will be controlled. Fig. 4C shows the SEM image at the cross-section of the CGAgMnB coating deposited on PB layers. It was inferred from Fig. 4C that

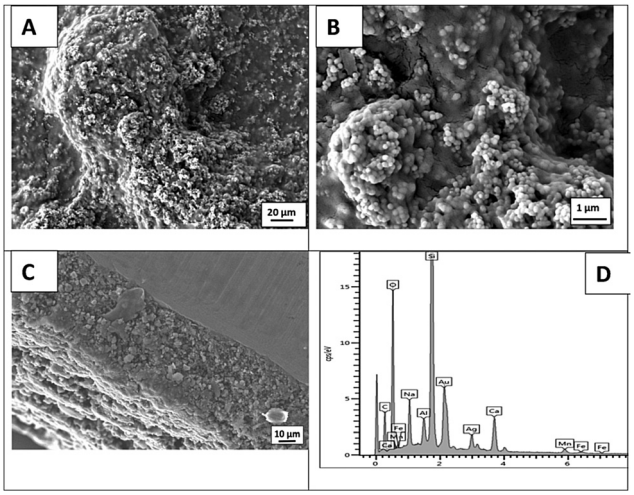

Fig. 4 SEM images and EDX analysis of the CGAgMnB coatings deposited on PB layers *via* EPD (applied voltage = 30 V, deposition time = 5 min): (A) SEM image from the top surface of the coatings at low magnification, (B) SEM image from the top surface of the coatings at higher magnification, (C) SEM image at the cross-section of the coatings, and (D) EDX analysis of the coatings.

the coating (CGAgMnB deposited on PB layers) thickness was ~70 μm. A similar coating thickness for PB based multi-structured coatings was reported in the literature.[26] It was not possible to measure the coating thickness of the two layers separately because the top layer did not show a clear interface with PB layers (Fig. 4C). Area EDX analysis of the multi-structured coatings revealed the presence of Mn, Ag, Ca, Na, and Si (Fig. 4D). The presence of Mn and Ag confirmed the presence of Ag–Mn MBGNs in the top layer. The Fe peak may be detected from the 316L SS substrate (Fig. 4D).

FTIR analysis. FTIR analysis of the multi-structured (CGAgMnB on PB layers) coatings was performed concerning the PB coatings and CGAgMnB coatings deposited on 316L SS (Fig. 5). It was observed that the FTIR spectrum of multi-structured coatings was similar to that of the CGAgMnB coatings deposited on 316L SS. The FTIR spectrum of multi-structured coatings showed the peaks attributed to chitosan, for example, stretching vibration in the C═O group at 1643 cm^{-1}, and N–H bending of amide II at 1543 cm^{-1} (amide-II).[19] The peaks attributed to gelatin were observed at 1170 cm^{-1} representing the stretching mode of vibration in the –COOH group.[19] Furthermore, it was observed that the representative peaks for chitosan and gelatin were superimposed on each other as peaks were overlapped at 1651 cm^{-1} (C═O[34,35]), 1536 cm^{-1} (C–H bonds[4]) and 1454 cm^{-1} (symmetrical stretching of the nitro group[36]) in the multi-structured coatings. The peaks relevant to PEEK were not depicted in the FTIR spectrum of the multi-structured coatings, which may be due to the fact that the PB layer was covered homogeneously by the CG layer. The presence of Ag–Mn MBGNs in the multi-structured coatings was indicated by the Si–O–Si bands at 565 cm^{-1}.[25]

The presence of Ag–Mn MBGNs was more evidentially confirmed by EDX analysis, as shown in Fig. 4D.

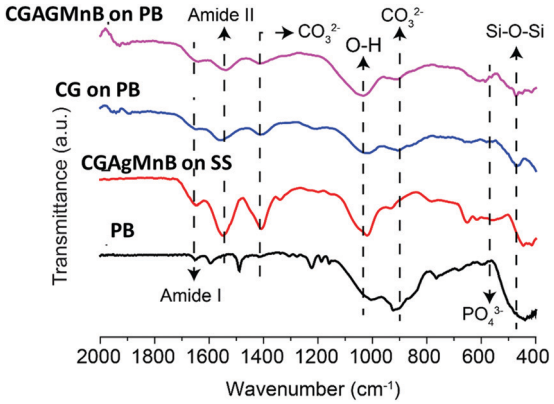

Fig. 5 FTIR spectrum of PEEK/BG coatings (labeled as PB), chitosan/gelatin/Ag–Mn MBGNs coatings on SS (labeled as CGAgMnB on SS), chitosan/gelatin coatings on the PEEK/BG layer (labeled as CG on PB), and chitosan/gelatin/Ag–Mn MBGNs coatings on the PEEK/BG layer (labeled as CGAgMnB on PB). The relevant peaks are discussed in the text.

3.6 Wettability

To determine the ability of the coatings to facilitate protein attachment, water contact angle measurements were carried out ten times on each set of samples. 316L SS, PB, and multi-structured coatings (CGAgMnB composite on PB layers) showed a contact angle of $86^\circ \pm 2^\circ$, $74 \pm 4^\circ$, and $50 \pm 4^\circ$, respectively. The wettability of the multi-structured coatings was in a suitable range for the proliferation and growth of osteoblast cells.[37] The contact angle of 50° for the multi-structured coatings was derived from the combination of the hydrophilic nature of bioactive glass particles and the hydrophobic nature of CG (polyelectrolyte complex).[19]

The ability of the surface of an implant to trigger a positive response from the human body is often governed by wettability (studied by water contact angle measurements), surface topography (studied by surface roughness measurements), and surface chemistry (studied by FTIR analysis). The ideal combination of these three properties may lead to enhanced protein attachment and proliferation of osteoblast and bone-marrow cells.[19,26]

3.7 Surface roughness

The surface topography influences the attachment of cells and bacteria. Thus, the surface roughness can affect the performance of the implant. Generally, osteoblast-like cells prefer roughness in the range of 1–2 μm. Furthermore, surface roughness can influence drug/metallic ion release in the physiological environment. Roughness measurement results showed that the average roughness for PB coatings was 2 ± 0.2 μm and for multi-structured coatings it was 1.2 ± 0.2 μm. The average roughness of multi-structured coatings was suitable for the attachment and proliferation of osteoblast-like cells. Similar values for the average roughness of PB based multi-structured coatings have been reported in the literature.[26]

3.8 *In vitro* bioactivity

The *in vitro* bioactivity test for the multi-structured coatings (CGAgMnB composite on PB layers) was carried out at 1, 3, 7, and 21 days of incubation. SEM images of the multi-structured coatings showed calcium phosphate formation on the surface after immersion in SBF (Fig. 4). As early as 1 day, HA formation was observed on the surface of the coatings, although only small nanoscale needles were observed (Fig. 6A and B). After 3 days of immersion in SBF, the coatings were covered with a cauliflower type structure of apatite, which is a qualitative representation of the bioactivity of coatings (Fig. 6C and D). After 7 days of immersion in SBF, the surface of the coatings showed a morphology similar to that at 3 days of incubation, as shown in Fig. S1A and B (Fig. S1, ESI†). After 21 days the surface of the coatings was completely covered with porous HA (Fig. 6E and F), which is excellent for osseointegration and osteoproduction.[1,38] The SEM micrographs showed that the size of apatite crystals was growing with the increase in immersion time.

The complete formation of calcium phosphate on coatings was confirmed by EDX measurements (Fig. 7). Fig. 7 shows that the intensity of the silicon peak decreases with the increase in the incubation period, which may be associated with the degradation of BG. Furthermore, the intensity of the phosphorus (P), carbon (C), and calcium (Ca) peaks tends to increase with the increase in the incubation period. The EDX results for the 3 and 7 days of immersion in SBF were similar. The EDX pattern for the multi-structured coatings after 7 days of immersion in SBF is shown in Fig. S1C (ESI†). The EDX results suggested that the carbonated HA mineral developed on the surface of the coatings (Ca, P, and C signal detected from HA).[1] The C signal in EDX spectra may be detected due to contamination. Therefore, the presence of C may not be the confirmation of carbonated HA. To confirm that carbonated HA is developed on the surface of the

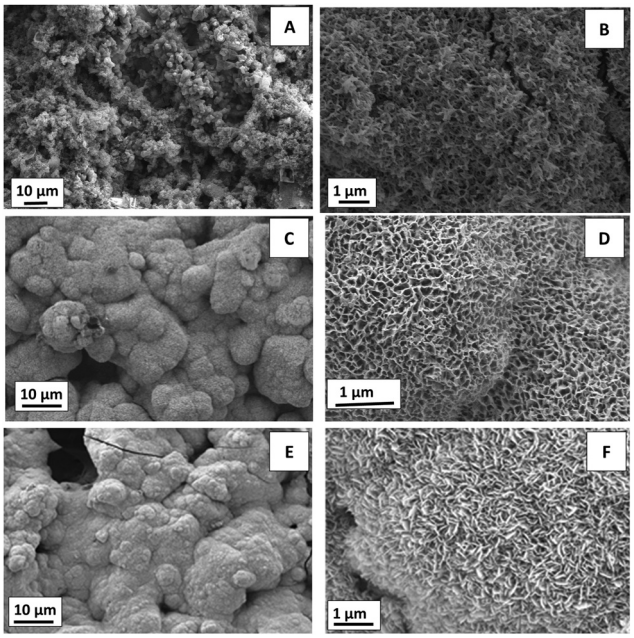

Fig. 6 SEM images of the CGAgMnB composite coating on PB layers after immersion in SBF for (A and B) 1 day, (C and D) 3 days, and (E and F) 21 days.

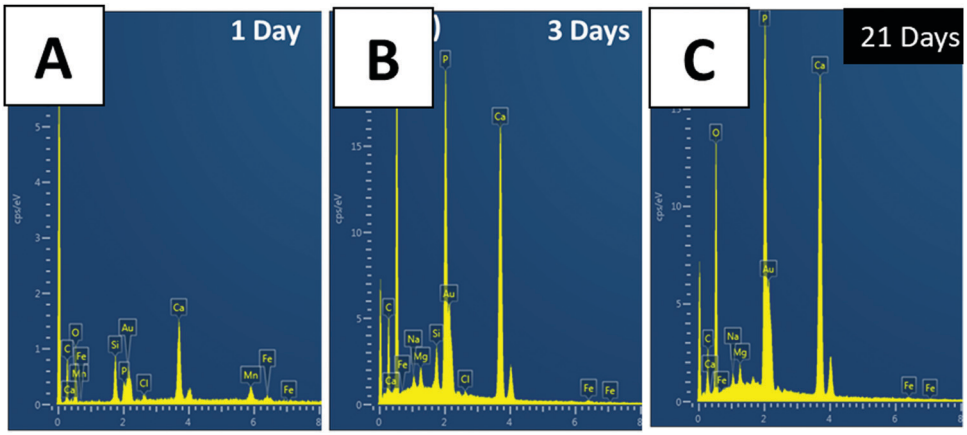

Fig. 7 EDX analysis of the CGAgMnB composite coating on PB layers after immersion in SBF for (A) 1 day, (B) 3 days, and (C) 21 days.

coatings FTIR analysis was done (Fig. 8A and the corresponding discussion). It was observed that a small amount of Mg substitution was present in the HA crystals, which was indicated by the presence of Mg peaks in Fig. 7. The calculated value for the Ca/P ratio after 21 days of incubation was 1.56 which is below the stoichiometric ratio of Ca/P for HA. The reason could be the substitution of Mg in the HA complex. SEM/EDX analysis of the multi-structured coatings after *in vitro* studies supported the bone binding ability of the coatings. HA crystals were observed on the surface of the coatings after just 1 day, which is a much better result in comparison to the literature.[3,39,40] The reason could be the presence of nanoscale bioactive particles on the top surface and the microscale BG in the bottom providing rapid ion exchange between the coatings and the physiological environment. Furthermore, the presence of CG polyelectrolyte complex aided favorable osteogenic response from the coatings. CGAgMnB is known to provide steric hindrance, which may be responsible for the accumulation of HA crystals on the top surface of the coatings.[6]

Fig. 8 represents the FTIR spectrum of the multi-structured coatings after incubation in SBF. It was deduced from Fig. 8 that the intensity of Si–O–Si bands (610 cm^{-1}) starts to decrease from 1 day to 21 days of treatment in SBF. Furthermore, the FTIR spectrum elucidated that new peaks emerged at 560 cm^{-1}, 610 cm^{-1} and 1014 cm^{-1} after SBF treatment. Upon comparison with the literature, it was found that these new peaks are attributed to phosphate groups.[41] The new peaks observed at 873 cm^{-1} and 1400 cm^{-1} after incubation in SBF were attributed to carbonate groups.[42] The emergence of new phosphate and carbonate bands in the FTIR spectrum after treatment in SBF confirmed that the crystals seen in the SEM images are of carbonate hydroxyapatite.[43]

The CG polyelectrolyte complex is expected to undergo degradation upon exposure to physiological conditions.[6] Accordingly, the FTIR spectrum (Fig. 8) after 1 day of incubation shows amide-I (1645 cm^{-1} [35]) and amide II (1558 cm^{-1} and 1406 cm^{-1} [35]) peaks. In contrast, after 3 days of incubation, the amide-I and amide-II regions appear to be a flat line, which is

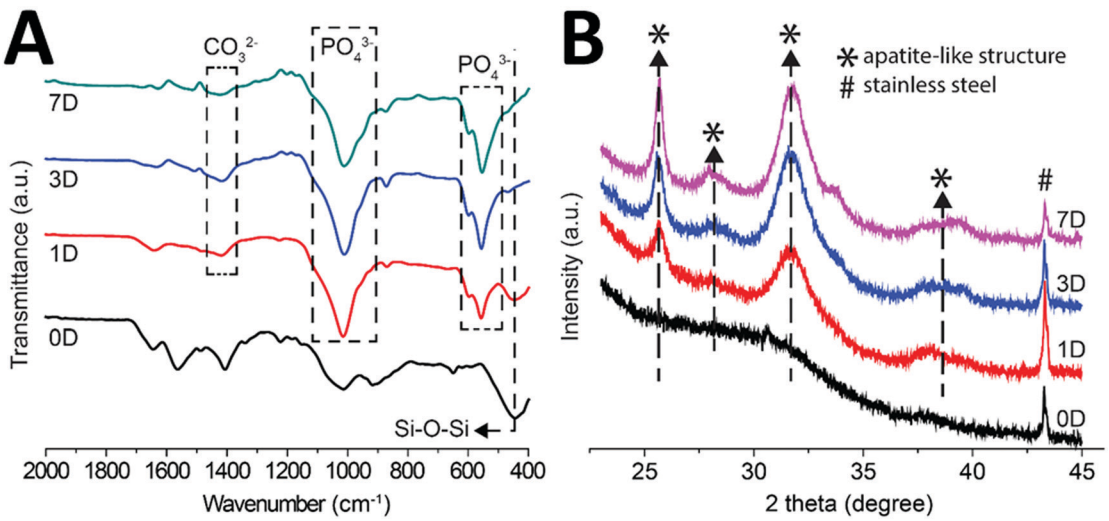

Fig. 8 (A) FTIR analysis of the multi-structured coatings before and after immersion in SBF for 1, 3, and 7 days, (B) XRD analysis of multi-structured coatings before and after immersion in SBF for 1, 3, and 7 days. PO.

an indication of the degradation of the CG complex and formation of HA crystals on the top surface of multi-structured coatings. These findings are consistent with the literature.[44]

Fig. 8B represents the XRD diffraction pattern of the coatings before and after immersion in SBF for 1, 3, and 7 days. It was observed that after immersion in SBF new peaks emerged at 2θ of $\sim 26^\circ$ and 32°, which is a qualitative indication of the formation of HA crystals on the surface of the coatings. Moreover, the diffraction peak at 2θ of 43° is a representation of the 316L SS substrate. It was observed that the intensity of the peaks attributed to HA increased with the increase in the immersion time, which indicates that the density of HA crystals is increasing with the increase in immersion time. The XRD results are in agreement with the FTIR, EDX, and SEM results. Thus, confirming that HA crystals are formed on the surface of the multi-structured coatings, which affirms the bone binding ability of the coatings.

The *in vitro* bioactivity studies for the PB coatings (control samples) showed the formations of HA crystals upon immersion in SBF after 1 day of incubation. The density of the HA crystals tends to increase with an increase in immersion time. The details of the *in vitro* bioactivity studies have recently been published.[29] CGAgMnB coatings deposited on 316L SS samples were also immersed in SBF but the formation of HA crystals was not observed even after one week of incubation (SEM image shown in Fig. S2, ESI†). Thus, it was concluded that the bioactivity of the multi-structured coatings was mainly attributed to the PB layer.

3.9 Antibacterial studies

The therapeutic effect associated with the release of silver ions was evaluated by tracking the antibacterial effect associated with the release of ions. The antibacterial effect of the CGAgMnB coatings on PB layers was studied by the agar disk diffusion test, as shown in Fig. 9. Fig. 9 shows that the CGAgMnB coatings on PB layers developed the zone of inhibition around the sample against Gram-positive (*S. carnosus*) and Gram-negative (*E. coli*) bacteria (Table 2). In contrast, PB (control sample) did not develop the zone of inhibition (figure not shown here). The antibacterial effect of chitosan/Ag Sr-HA coatings was thus attributed to the release of silver. However, in this study, the release of silver ions was not evaluated quantitatively, and thus, it will be an important task for the future.

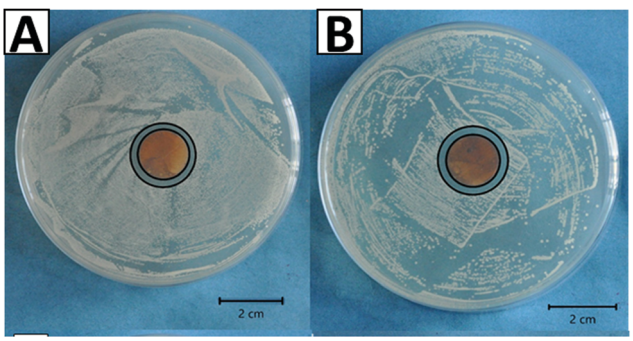

Fig. 9 Inhibition halo tests for the multi-structured coatings with (A) *E. coli* and (B) *S. carnosus*.

Table 2 Antibacterial disc susceptibility tests showing relative diameters of inhibition for the multi-structured coatings and the PB layers

	Zone of inhibition halo (mm) against	
Material	*E. coli*	*S. carnosus*
PEEK/BG	0 mm	0 mm
Multi-structured coatings	2.1 ± 0.2 mm	2.3 ± 0.2 mm

The antibacterial effect of the coatings is associated with the release of silver in an ionic form. The silver changes to ionic form upon exposure to the physiological medium. The ionic silver is highly reactive to the electron donor species. Thus, the ionic silver may rupture the walls of the bacteria and enter into the membrane hindering the DNA replication activity, which may lead to the death of the bacteria.[24,33]

3.10 *In vitro* cellular studies

The cellular metabolic activity of the CG and CGAgMnB coatings on PB layers was measured by the WST-8 assay based on the percentage of cell viability. Fig. 10 shows that the CG and CGAgMnB coatings on PB layers supported the proliferation of human osteoblast-like cells(MG-63) for 2 days. The cell viability (%) difference between the tissue culture plate (positive control) and the multilayer coatings with and without silver was insignificant at $p < 0.05$. Moreover, Fig. 10 suggests that the incorporation of Ag in the multilayer coatings did not lead to a cytotoxic effect, as the difference in the cell viability (%) of the two multilayer coatings (with and without Ag) was statistically insignificant (Fig. 10). A similar behavior of chitosan/BG/gentamicin has already been reported by Pishbin *et al.*[3] It was hypothesized that any cytotoxic effect associated with the release of silver ions will be

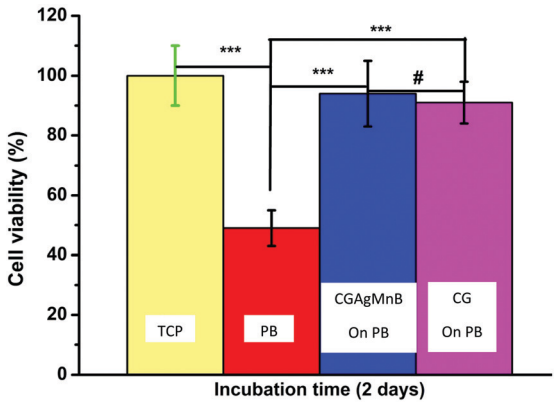

Fig. 10 The response of human osteoblast-like cells (MG-63) to PB coatings, CGAgMnB on PB, and CG coatings on PB layers measured by WST-8 up to 2 days of culture. TCP was used as control. The resultant number of cells for each coating was normalized against the number of cells on a tissue culture plate on a particular day. *** denotes that the difference between two systems is significant at $p < 0.001$ and # denotes that the difference between two systems is insignificant at $p < 0.05$ (data represent the mean ± standard deviation of two individual experiments each performed in pentaplicate).

mitigated by the release of Mn ions. It has been reported in the literature that Mn enhances the osteogenic response of MBGNs.[16,45]

The density and distribution of the cells on the surface of CGAgMnB and CG coatings on PB layers were evaluated by fluorescence microscopy (Fig. 11). Calcein/DAPI fluorescent staining is generally used to indicate intracellular esterase activity present in viable cells.[46–48] Dense and evenly dispersed cells with relatively large nuclei were observed on the surface of both coatings, as shown in Fig. 11A and B. Moreover, CGAgMnB and CG coatings on PB layers exhibited a large number of living cells on their surfaces. The results of fluorescence microscopy are coherent with the cell viability test (WST-8 assay). Fluorescence microscopy images show that the CGAgMnB coatings on PB layers cause no adverse effect on the growth of MG-63 cells after 2 days of cultivation (compared to the CG coatings), which confirms the non-toxic behavior of Ag in the multi-structured coatings. The good dispersion and attachment of cells on both types of coatings may be due to the hydrophilic nature of the coatings, which allows the MG-63 cells to adhere to the surface of coatings.[49,50] Furthermore, controlled roughness ($R_a \sim 1.3$ μm) of the coatings allows the cells to spread over the whole surface. Recently, Ureña *et al.*[51] showed the favorable viability and attachment of ST-2 cells on Ti–Nb surfaces, which were modified to achieve the average roughness in the range of 1.38–1.80 μm. We conclude based on fluorescence microscopy and cell viability test that CGAgMnB coatings persisted and enhanced osteoblastic attachment and proliferation, which could be due to the surface topography, release of ions (dissolution products) from MBGNs and the release of gelatin.[52–54] Moreover, the presence of gelatin can increase degradation behavior which might reduce the steric hindrance on the encapsulated cells, enabling them to grow and proliferate.[55]

Cell morphology is correlated with important biochemical functions of cells such as adhesion, proliferation, and migration.[56] The morphology of MG-63 cells adhered to the surface of CGAgMnB coatings was investigated by SEM over the cultivation period (Fig. 12). Fig. 12 shows that the cells were elongated and adopted a strong cell–matrix adhesion and guided morphology due to the highly adhesive protein content. The higher degradation rate of the CG matrix led to a porous structure on the surface of coatings due to which embedded cells might experience low steric hindrance.[55]

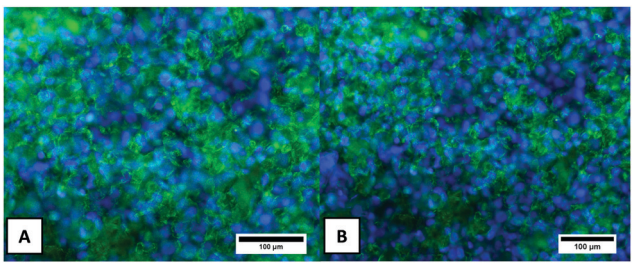

Fig. 11 Fluorescence microscopy images of MG-63 cells cultured on different samples stained with Calcein and DAPI after 2 days (live cell staining in green and nuclei in blue): (A) CGAgMnB coatings on PB layers and (B) CG coatings on PB layers.

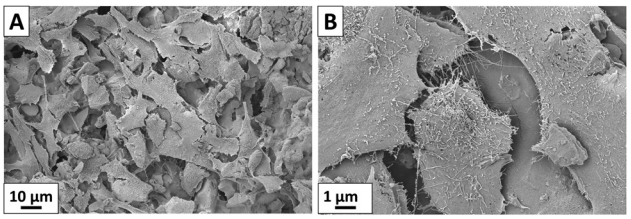

Fig. 12 SEM images showing the morphology of MG-63 cells spreading on the surface of CGAgMnB coatings on PB layers after 2 days of incubation in cell culture medium: (A) at low magnification and (B) at high magnification.

Several studies have reported that the incorporation of cell-binding peptides, specifically RGD, improves the osteogenic differentiation of progenitor or osteoblast cell.[57,58] Since gelatin possesses the RGD sequence of collagen,[59,60] the presence of RGD peptide in the coatings can stimulate the activity of cell integrin receptors that may play a role in osteogenic differentiation. Moreover, the presence of gelatin can enhance cell viability, cell spreading with interconnected networks, and osteogenic differentiation. All these confirm the suitability of CGAgMnB coatings on PB layers for bone tissue engineering applications.

4. Conclusions

The Taguchi design of experiment approach (DoE) was used to optimize CGAgMnB coatings on 316L SS *via* EPD. PB composite coatings deposited on 316 L SS provided an effective platform for the deposition of CGAgMnB composite coatings *via* EPD. SEM and FTIR analysis showed the successful deposition of CGAgMnB on PB layers. Moreover, the presence of Ag and Mn was confirmed by EDX analyses. SEM images of multi-structured coatings showed that the CGAgMnB coating spread on the surface of the PB layer and filled its porous structure to various extents due to variations in the surface roughness of the PB layers. Multi-structured coatings showed the formation of HA crystals after 1 day of immersion in SBF, which indicates the bioactive behavior of the coatings. Multi-structured coatings exhibit antibacterial activity against Gram-positive and Gram-negative bacteria. Furthermore, *in vitro* cellular studies elucidated that the presence of gelatin and Mn in multi-structured coatings enhanced the cell viability, cell attachment, and cell spreading. WST-8 assay and fluorescence microscopy confirmed the non-toxic behavior of CGAgMnB coatings. All these results confirm the suitability of CGAgMnB coatings on PB for bone tissue engineering applications.

This research work may pave the way for multi-structured coatings to be considered for *in vivo* tests and clinical trials. However, it is pertinent to mention that long-term silver release tests, antibacterial tests, and cell viability tests should be done before any further consideration.

Conflicts of interest

The authors declare no competing financial interest and there is no conflict of interest to disclose.

Acknowledgements

MAUR would like to acknowledge the Higher Education Commission of Pakistan for the award of the SRGP grant. The authors would like to thank Mr Tahir Khan for SEM analysis and Dr Ibrahim Qazi (HoD) Materials Science and Engineering for providing free access to all the instruments at Institute of Space Technology, Islamabad, Pakistan.

References

1 M. A. Ur Rehman, S. Ferraris, W. H. Goldmann, S. Perero, F. E. Bastan, Q. Nawaz, G. G. Confiengo, M. Ferraris and A. R. Boccaccini, Antibacterial and Bioactive Coatings Based on Radio Frequency Co-Sputtering of Silver Nanocluster-Silica Coatings on PEEK/Bioactive Glass Layers Obtained by Electrophoretic Deposition, *ACS Appl. Mater. Interfaces*, 2017, **9**(38), 32489–32497, DOI: 10.1021/acsami.7b08646.

2 A. Simchi, E. Tamjid, F. Pishbin and A. R. Boccaccini, Recent Progress in Inorganic and Composite Coatings with Bactericidal Capability for Orthopaedic Applications, *Nanomedicine*, 2011, **7**(1), 22–39, DOI: 10.1016/j.nano.2010.10.005.

3 F. Pishbin, V. Mouriño, S. Flor, S. Kreppel, V. Salih, M. P. Ryan and A. R. Boccaccini, Electrophoretic Deposition of Gentamicin-Loaded Bioactive Glass/Chitosan Composite Coatings for Orthopaedic Implants, *ACS Appl. Mater. Interfaces*, 2014, **6**(11), 8796–8806, DOI: 10.1021/am5014166.

4 F. Pishbin, V. Mouriño, J. B. Gilchrist, D. W. McComb, S. Kreppel, V. Salih, M. P. Ryan and A. R. Boccaccini, Single-Step Electrochemical Deposition of Antimicrobial Orthopaedic Coatings Based on a Bioactive Glass/Chitosan/Nano-Silver Composite System, *Acta Biomater.*, 2013, **9**(7), 7469–7479, DOI: 10.1016/j.actbio.2013.03.006.

5 A. R. Boccaccini, S. Keim, R. Ma, Y. Li and I. Zhitomirsky, Electrophoretic Deposition of Biomaterials, *J. R. Soc., Interface*, 2010, **7**(Suppl. 5 (May)), S581–S613, DOI: 10.1098/rsif.2010.0156.focus.

6 E. Avcu, F. E. Baştan, H. Z. Abdullah, M. A. Ur Rehman, Y. Yıldıran Avcu and A. R. Boccaccini, Electrophoretic Deposition of Chitosan-Based Composite Coatings for Biomedical Applications: A Review, *Prog. Mater. Sci.*, 2019, **103**(January), 69–108, DOI: 10.1016/j.pmatsci.2019.01.001.

7 S. Seuss, M. Heinloth and A. R. Boccaccini, Development of Bioactive Composite Coatings Based on Combination of PEEK, Bioactive Glass and Ag Nanoparticles with Antibacterial Properties, *Surf. Coat. Technol.*, 2015, **301**, 100–105, DOI: 10.1016/j.surfcoat.2016.03.057.

8 Q. Nawaz, M. A. U. Rehman, A. Burkovski, J. Schmidt, A. M. Beltrán, A. Shahid, N. K. Alber, W. Peukert and A. R. Boccaccini, Synthesis and Characterization of Manganese Containing Mesoporous Bioactive Glass Nanoparticles for Biomedical Applications, *J. Mater. Sci.: Mater. Med.*, 2018, **5**, 64, DOI: 10.1007/s10856-018-6070-4.

9 C. Wu, Y. Zhou, C. Lin, J. Chang and Y. Xiao, Strontium-Containing Mesoporous Bioactive Glass Scaffolds with Improved Osteogenic/Cementogenic Differentiation of Periodontal Ligament Cells for Periodontal Tissue Engineering, *Acta Biomater.*, 2012, **8**(10), 3805–3815, DOI: 10.1016/j.actbio.2012.06.023.

10 A. J. Salinas, S. Shruti, G. Malavasi, L. Menabue and M. Vallet-Regí, Substitutions of Cerium, Gallium and Zinc in Ordered Mesoporous Bioactive Glasses, *Acta Biomater.*, 2011, **7**(9), 3452–3458, DOI: 10.1016/j.actbio.2011.05.033.

11 J. Ye, J. He, C. Wang, K. Yao and Z. Gou, Copper-Containing Mesoporous Bioactive Glass Coatings on Orbital Implants for Improving Drug Delivery Capacity and Antibacterial Activity, *Biotechnol. Lett.*, 2014, **36**(5), 961–968, DOI: 10.1007/s10529-014-1465-x.

12 C. Wu and J. Chang, Multifunctional Mesoporous Bioactive Glasses for Effective Delivery of Therapeutic Ions and Drug/Growth Factors, *J. Controlled Release*, 2014, **193**, 282–295, DOI: 10.1016/j.jconrel.2014.04.026.

13 W. Xia and J. Chang, Well-Ordered Mesoporous Bioactive Glasses (MBG): A Promising Bioactive Drug Delivery System, *J. Controlled Release*, 2006, **110**(3), 522–530, DOI: 10.1016/j.jconrel.2005.11.002.

14 S. Kaya, M. Cresswell and A. R. Boccaccini, Mesoporous Silica-Based Bioactive Glasses for Antibiotic-Free Antibacterial Applications, *Mater. Sci. Eng., C*, 2018, **83**(August 2017), 99–107, DOI: 10.1016/j.msec.2017.11.003.

15 A. Philippart, N. Gómez-Cerezo, D. Arcos, A. J. Salinas, E. Boccardi, M. Vallet-Regi and A. R. Boccaccini, Novel Ion-Doped Mesoporous Glasses for Bone Tissue Engineering: Study of Their Structural Characteristics Influenced by the Presence of Phosphorous Oxide, *J. Non-Cryst. Solids*, 2017, **455**, 90–97, DOI: 10.1016/j.jnoncrysol.2016.10.031.

16 F. Westhauser, S. Wilkesmann, Q. Nawaz, S. I. Schmitz, A. Moghaddam and A. R. Boccaccini, Osteogenic Properties of Manganese-Doped Mesoporous Bioactive Glass Nanoparticles, *J. Biomed. Mater. Res., Part A*, 2020, **108**(9), 1806–1815, DOI: 10.1002/jbm.a.36945.

17 A. A. El-Rashidy, G. Waly, A. Gad, A. A. Hashem, P. Balasubramanian, S. Kaya, A. R. Boccaccini and I. Sami, Preparation and in Vitro Characterization of Silver-Doped Bioactive Glass Nanoparticles Fabricated Using a Sol-Gel Process and Modified Stöber Method, *J. Non-Cryst. Solids*, 2018, **483**, 26–36, DOI: 10.1016/j.jnoncrysol.2017.12.044.

18 K. Zheng and A. R. Boccaccini, Sol-Gel Processing of Bioactive Glass Nanoparticles: A Review, *Adv. Colloid Interface Sci.*, 2017, **249**, 363–373, DOI: 10.1016/j.cis.2017.03.008.

19 M. A. U. Rehman, M. A. Munawar, D. W. Schubert and A. R. Boccaccini, Electrophoretic Deposition of Chitosan/Gelatin/Bioactive Glass Composite Coatings on 316L Stainless Steel: A Design of Experiment Study, *Surf. Coat. Technol.*, 2019, **358**(November 2018), 976–986, DOI: 10.1016/j.surfcoat.2018.12.013.

20 R. Chen, X. Cai, K. Ma, Y. Zhou, Y. Wang and T. Jiang, The Fabrication of Double-Layered Chitosan/Gelatin/Genipin Nanosphere Coating for Sequential and Controlled Release of Therapeutic Proteins, *Biofabrication*, 2017, **7**(2), 025028, DOI: 10.1088/1758-5090/aa70c3.

21 J. Song, Q. Chen, Y. Zhang, M. Diba, E. Kolwijck, J. Shao, J. A. Jansen, F. Yang, A. R. Boccaccini and S. C. G. Leeuwenburgh, Electrophoretic Deposition of Chitosan Coatings Modified with Gelatin Nanospheres to Tune the Release of Antibiotics, *ACS Appl. Mater. Interfaces*, 2016, **8**(22), 13785–13792, DOI: 10.1021/acsami.6b03454.

22 J. S. Mao, Y. L. Cui, X. H. Wang, Y. Sun, Y. J. Yin, H. M. Zhao and K. De Yao, A Preliminary Study on Chitosan and Gelatin Polyelectrolyte Complex Cytocompatibility by Cell Cycle and Apoptosis Analysis, *Biomaterials*, 2004, **25**(18), 3973–3981, DOI: 10.1016/j.biomaterials.2003.10.080.

23 T. Moskalewicz, S. Seuss and A. R. Boccaccini, Microstructure and Properties of Composite Polyetheretherketone/Bioglass® Coatings Deposited on Ti–6Al–7Nb Alloy for Medical Applications, *Appl. Surf. Sci.*, 2013, **273**, 62–67, DOI: 10.1016/j.apsusc.2013.01.174.

24 M. Miola, E. Vernè, A. Piredda, S. Seuss, S. Cabanas-Polo and A. R. Boccaccini, Development and Characterization of PEEK/B_2O_3-Doped 45S5 Bioactive Glass Composite Coatings Obtained by Electrophoretic Deposition, *Key Eng. Mater.*, 2015, **654**, 3–7, DOI: 10.4028/www.scientific.net/KEM.654.165.

25 M. A. U. Rehman, F. E. Bastan, B. Haider and A. R. Boccaccini, Electrophoretic Deposition of PEEK/Bioactive Glass Composite Coatings for Orthopedic Implants: A Design of Experiments (DoE) Study, *Mater. Des.*, 2017, **130**(March), 223–230, DOI: 10.1016/j.matdes.2017.05.045.

26 M. A. U. Rehman, F. E. Bastan, Q. Nawaz, W. H. Goldmann, M. Maqbool, S. Virtanen and A. R. Boccaccini, Electrophoretic Deposition of Lawsone Loaded Bioactive Glass (BG)/Chitosan Composite on Polyetheretherketone (PEEK)/BG Layers as Antibacterial and Bioactive Coating, *J. Biomed. Mater. Res., Part A*, 2018, 1–12, DOI: 10.1002/jbm.a.36506.

27 R. S. Virk, M. A. U. Rehman, M. A. Munawar, D. W. Schubert, W. H. Goldmann, J. Dusza and A. R. Boccaccini, Curcumin-Containing Orthopedic Implant Coatings Deposited on Poly-Ether-Ether-Ketone/Bioactive Glass/Hexagonal Boron Nitride Layers by Electrophoretic Deposition, *Coatings*, 2019, **9**, 572.

28 M. A. U. Rehman, F. E. Bastan, Q. Nawaz, A. R. Boccaccini, M. A. U. Rehman, F. E. Bastan, Q. Nawaz, A. R. Boccaccini, M. Atiq, U. Rehman, F. E. Bastan, Q. Nawaz and A. R. Boccaccini, Electrophoretic Deposition of Lawsone Loaded Nanoscale Silicate Glass/Chitosan Composite on PEEK/BG Layers, *Electrochem. Soc. Trans.*, 2018, **82**(1), 45–50, DOI: 10.1149/08201.0045ecst.

29 M. A. U. Rehman, F. E. Bastan, A. Nawaz, Q. Nawaz and A. Wadood, Electrophoretic deposition of PEEK/bioactive glass composite coatings on stainless steel for orthopedic applications: an optimization for *in vitro* bioactivity and adhesion strength, *Int. J. Adv. Manu. Technol.*, 2020, **108**, 1849–1862.

30 L. Besra and M. Liu, A Review on Fundamentals and Applications of Electrophoretic Deposition (EPD), *Prog. Mater. Sci.*, 2007, **52**(1), 1–61, DOI: 10.1016/j.pmatsci.2006.07.001.

31 L. L. Hench, The Story of Bioglass®, *J. Mater. Sci.: Mater. Med.*, 2006, **17**(11), 967–978, DOI: 10.1007/s10856-006-0432-z.

32 T. Kokubo and H. Takadama, How Useful Is SBF in Predicting *in Vivo* Bone Bioactivity?, *Biomaterials*, 2006, **27**(15), 2907–2915, DOI: 10.1016/j.biomaterials.2006.01.017.

33 J. Ballarre, T. Aydemir, L. Liverani, J. A. Roether, W. H. Goldmann and A. R. Boccaccini, Versatile Bioactive and Antibacterial Coating System Based on Silica, Gentamicin, and Chitosan: Improving Early Stage Performance of Titanium Implants, *Surf. Coat. Technol.*, 2020, **381**, 125–138, DOI: 10.1016/j.surfcoat.2019.125138.

34 D. Rajeswari, D. Gopi, S. Ramya and L. Kavitha, Investigation of Anticorrosive, Antibacterial and *in Vitro* Biological Properties of a Sulphonated Poly(Etheretherketone)/Strontium, Cerium Co-Substituted Hydroxyapatite Composite Coating Developed on Surface Treated Surgical Grade Stainless Steel for Orth, *RSC Adv.*, 2014, **4**(106), 61525–61536, DOI: 10.1039/c4ra12207k.

35 Z. Zhang, X. Cheng, Y. Yao, J. Luo, Q. Tang, H. Wu, S. Lin, C. Han, Q. Wei and L. Chen, Electrophoretic Deposition of Chitosan/Gelatin Coatings with Controlled Porous Surface Topography to Enhance Initial Osteoblast Adhesive Responses, *J. Mater. Chem. B*, 2016, **4**(47), 7584–7595, DOI: 10.1039/C6TB02122K.

36 Y. Wang, X. Guo, R. Pan, D. Han, T. Chen, Z. Geng, Y. Xiong and Y. Chen, Electrodeposition of Chitosan/Gelatin/Nanosilver: A New Method for Constructing Biopolymer/Nanoparticle Composite Films with Conductivity and Antibacterial Activity, *Mater. Sci. Eng., C*, 2015, **53**, 222–228, DOI: 10.1016/j.msec.2015.04.031.

37 K. L. Menzies and L. Jones, The Impact of Contact Angle on the Biocompatibility of Biomaterials, *Optom. Vis. Sci.*, 2010, **87**(6), 387–399, DOI: 10.1097/OPX.0b013e3181da863e.

38 A. Stoch, W. Jastrzębski, A. Brożek, B. Trybalska, M. Cichocińska and E. Szarawara, FTIR Monitoring of the Growth of the Carbonate Containing Apatite Layers from Simulated and Natural Body Fluids, *J. Mol. Struct.*, 1999, **511**, 287–294, DOI: 10.1016/S0022-2860(99)00170-2.

39 M. Miola, E. Verné, F. E. Ciraldo, L. Cordero-Arias and A. R. Boccaccini, Electrophoretic Deposition of Chitosan/45S5 Bioactive Glass Composite Coatings Doped with Zn and Sr, *Front. Bioeng. Biotechnol.*, 2015, **3**, 159, DOI: 10.3389/fbioe.2015.00159.

40 N. S. Raddaha, L. Cordero-Arias, S. Cabanas-Polo, S. Virtanen, J. A. Roether and A. R. Boccaccini, Electrophoretic Deposition of Chitosan/h-BN and Chitosan/h-BN/TiO_2 Composite Coatings on Stainless Steel (316L) Substrates, *Materials*, 2014, **7**(3), 1814–1829, DOI: 10.3390/ma7031814.

41 S. Seuss, M. Lehmann and A. R. Boccaccini, Alternating Current Electrophoretic Deposition of Antibacterial Bioactive Glass-Chitosan Composite Coatings, *Int. J. Mol. Sci.*, 2014, **15**(7), 12231–12242, DOI: 10.3390/ijms150712231.

42 R. Torkaman, S. Darvishi, M. Jokar, M. Kharaziha and M. Karbasi, Electrochemical and *in Vitro* Bioactivity of Nanocomposite Gelatin-Forsterite Coatings on AISI 316 L

Stainless Steel, *Prog. Org. Coat.*, 2017, **103**, 40–47, DOI: 10.1016/j.porgcoat.2016.11.029.

43 J. H. Kim, S. H. Kim, H. K. Kim, T. Akaike and S. C. Kim, Synthesis and Characterization of Hydroxyapatite Crystals: A Review Study on the Analytical Methods, *J. Biomed. Mater. Res.*, 2002, **62**(4), 600–612, DOI: 10.1002/jbm.10280.

44 K. Ma, X. Cai, Y. Zhou, Z. Zhang, T. Jiang and Y. Wang, Osteogenetic Property of a Biodegradable Three-Dimensional Macroporous Hydrogel Coating on Titanium Implants Fabricated *via* EPD, *Biomed. Mater.*, 2014, **9**(1), 15008, DOI: 10.1088/1748-6041/9/1/015008.

45 Q. Nawaz, M. A. U. Rehman, J. A. Roether, L. Yufei, A. Grünewald, R. Detsch and A. R. Boccaccini, Bioactive Glass Based Scaffolds Incorporating Gelatin/Manganese Doped Mesoporous Bioactive Glass Nanoparticle Coating, *Ceram. Int.*, 2019, **45**(12), 14608–14613, DOI: 10.1016/j.ceramint.2019.04.179.

46 M. Furko, V. Havasi, Z. Kónya, A. Grünewald, R. Detsch, A. R. Boccaccini and C. Balázsi, Development and Characterization of Multi-Element Doped Hydroxyapatite Bioceramic Coatings on Metallic Implants for Orthopedic Applications, *Bol. Soc. Esp. Ceram. Vidrio*, 2017, 1–11, DOI: 10.1016/j.bsecv.2017.09.003.

47 Y. Yang, K. Zheng, R. Liang, A. Mainka, N. Taccardi, J. A. Roether, R. Detsch, W. H. Goldmann, S. Virtanen and A. R. Boccaccini, Cu-Releasing Bioactive Glass/Polycaprolactone Coating on Mg with Antibacterial and Anticorrosive Properties for Bone Tissue Engineering, *Biomed. Mater.*, 2018, **13**(1), 15001, DOI: 10.1088/1748-605X/aa87f2.

48 Y. Yang, J. Zhou, R. Detsch, N. Taccardi, S. Heise, S. Virtanen and A. R. Boccaccini, Biodegradable Nanostructures: Degradation Process and Biocompatibility of Iron Oxide Nanostructured Arrays, *Mater. Sci. Eng., C*, 2018, **85**(March 2017), 203–213, DOI: 10.1016/j.msec.2017.12.021.

49 H. K. Kim, J. W. Jang and C. H. Lee, Surface Modification of Implant Materials and Its Effect on Attachment and Proliferation of Bone Cells, *J. Mater. Sci.: Mater. Med.*, 2004, **15**(7), 825–830, DOI: 10.1023/B:JMSM.0000032824.62866.a1.

50 N. S. Radda'a, W. H. Goldmann, R. Detsch, J. A. Roether, L. Cordero-Arias, S. Virtanen, T. Moskalewicz and A. R. Boccaccini, Electrophoretic Deposition of Tetracycline Hydrochloride Loaded Halloysite Nanotubes Chitosan/Bioactive Glass Composite Coatings for Orthopedic Implants, *Surf. Coat. Technol.*, 2017, **327**, 146–157, DOI: 10.1016/j.surfcoat.2017.07.048.

51 J. Ureña, S. Tsipas, A. Jiménez-Morales, E. Gordo, R. Detsch and A. R. Boccaccini, Cellular Behaviour of Bone Marrow Stromal Cells on Modified Ti–Nb Surfaces, *Mater. Des.*, 2018, **140**, 452–459, DOI: 10.1016/j.matdes.2017.12.006.

52 B. Sarker, D. G. Papageorgiou, R. Silva, T. Zehnder, F. Gul-E-Noor, M. Bertmer, J. Kaschta, K. Chrissafis, R. Detsch and A. R. Boccaccini, Fabrication of Alginate–Gelatin Crosslinked Hydrogel Microcapsules and Evaluation of the Microstructure and Physico-Chemical Properties, *J. Mater. Chem. B*, 2014, **2**(11), 1470, DOI: 10.1039/c3tb21509a.

53 A. Grigore, B. Sarker, B. Fabry, A. R. Boccaccini and R. Detsch, Behavior of Encapsulated MG-63 Cells in RGD and Gelatine-Modified Alginate Hydrogels, *Tissue Eng., Part A*, 2014, **20**(15–16), 2140–2150, DOI: 10.1089/ten.tea.2013.0416.

54 Q. Chen, R. P. Garcia, J. Munoz, U. Pérez De Larraya, N. Garmendia, Q. Yao and A. R. Boccaccini, Cellulose Nanocrystals-Bioactive Glass Hybrid Coating as Bone Substitutes by Electrophoretic Co-Deposition: *In Situ* Control of Mineralization of Bioactive Glass and Enhancement of Osteoblastic Performance, *ACS Appl. Mater. Interfaces*, 2015, **7**(44), 24715–24725, DOI: 10.1021/acsami.5b07294.

55 B. Sarker, T. Zehnder, S. N. Rath, R. E. Horch, U. Kneser, R. Detsch and A. R. Boccaccini, Oxidized Alginate–Gelatin Hydrogel: A Favorable Matrix for Growth and Osteogenic Differentiation of Adipose-Derived Stem Cells in 3D, *ACS Biomater. Sci. Eng.*, 2017, **3**(8), 1730–1737, DOI: 10.1021/acsbiomaterials.7b00188.

56 W. Hassan, Y. Dong and W. Wang, Encapsulation and 3D Culture of Human Adipose-Derived Stem Cells in an *in Situ* Crosslinked Hybrid Hydrogel Composed of PEG-Based Hyperbranched Copolymer and Hyaluronic Acid, *Stem Cell Res. Ther.*, 2013, **4**(2), 1, DOI: 10.1186/scrt182.

57 H. Shin, K. Zygourakis, M. C. Farach-Carson, M. J. Yaszemski and A. G. Mikos, Modulation of Differentiation and Mineralization of Marrow Stromal Cells Cultured on Biomimetic Hydrogels Modified with Arg–Gly–Asp Containing Peptides, *J. Biomed. Mater. Res.*, 2004, **69A**(3), 535–543, DOI: 10.1002/jbm.a.30027.

58 Z. Qu, J. Yan, B. Li, J. Zhuang and Y. Huang, Improving Bone Marrow Stromal Cell Attachment on Chitosan/Hydroxyapatite Scaffolds by an Immobilized RGD Peptide, *Biomed. Mater.*, 2010, **5**(6), DOI: 10.1088/1748-6041/5/6/065001.

59 B. Sarker, R. Singh, R. Silva, J. A. Roether, J. Kaschta, R. Detsch, D. W. Schubert, I. Cicha and A. R. Boccaccini, Evaluation of Fibroblasts Adhesion and Proliferation on Alginate-Gelatin Crosslinked Hydrogel, *PLoS One*, 2014, **9**(9), 1–12, DOI: 10.1371/journal.pone.0107952.

60 E. Rosellini, C. Cristallini, N. Barbani, G. Vozzi and P. Giusti, Preparation and Characterization of Alginate/Gelatin Blend Films for Cardiac Tissue Engineering, *J. Biomed. Mater. Res., Part A*, 2009, **91**(2), 447–453, DOI: 10.1002/jbm.a.32216.